Supplement of Atmos. Chem. Phys., 24, 2639–2649, 2024
https://doi.org/10.5194/acp-24-2639-2024-supplement

Atmospheric Chemistry and Physics
Open Access

Supplement of

Molecular analysis of secondary organic aerosol and brown carbon from the oxidation of indole

Feng Jiang et al.

Correspondence to: Feng Jiang (feng.jiang@kit.edu) and Harald Saathoff (harald.saathoff@kit.edu)

List of Figures

Figure S1. Schematic of the AIDA simulation chamber and its instrumentation employed for this study. 12

Figure S2. Evolution of trace gases, light absorption, particle mass, and size distribution of indole oxidation at REF. (a), AS (b), and AS-NO_2 (c).....13

Figure S3. Indole calibration plot for PTR-MS measurements: normalized signals at 118.15 m/z (ncps) vs. generated mixing ratio (ppbv) 14

Figure S4. Organic mass concentration from SMPS measurement and COSIMA model (a reference experiment), including organic mass from SMPS (black points), organic mass from COSIMA model (red points), gas wall mass (brown line), and particle wall loss (blue line).....15

Figure S5. Organic mass concentration from SMPS measurement and COSIMA model (a seed particle experiment), including organic mass from SMPS (black points), organic mass from COSIMA model (red points), gas wall mass (brown line), and particle wall loss (blue line). 16

Figure S6. Yields of *ind*-SOA during stable period were recorded in the REF (pink), AS (green), and AS-NO_2 (black) experiments. The blue bar shows previously reported data by Montoya-Aguilera et al. (2017). The yields were calculated under stable periods for one hour (plateau level).....17

Figure S7. $MAC_{405\ online}$ of *ind*-SOA during the three experiments measured by a photoacoustic spectrometer. AS-NO_2 (black), AS (green), and REF (pink).....18

Figure S8. High-resolution AMS mass spectra of ind-SOA generated in the REF., AS, and NO_2-AS experiments. The major ion groups are grouped for clarity as Cx (black), CH+ (dark green), CHO1 (green), CHOgt1 (pink), and CHN (purple). 19

Figure S9. Molecular characteristics of individual components of *ind*-SOA identified in the reference sample. Panel (a) is the normalization of UPLC-PDA chromatograms and identified chromophores. Panel (b) shows a compilation of the selected extracted ion chromatograms (EICs) and the molecular structure of the most abundant peaks. Panel (c) shows the MAC from UV-visible spectrometer and UPLC-PDA measurement and absorption fractions. Unresolved chromophores (grey), unassigned chromophores (black), and $C_8H_7O_3N$ (green).....20

Figure S10. Thermograms of $C_8H_6O_2N_2$, $C_8H_7O_4N$, $C_8H_7O_3N$, and $C_8H_5O_3N$. Please note that broader thermograms, like those of $C_8H_7O_4N$, $C_8H_7O_3N$, and especially $C_8H_5O_3N$, may be caused by the presence of isomers of different volatility and thermal decomposition of larger molecules. Furthermore, the thermograms are also influenced by the overall composition of the matrix on the filter e.g. the ratio of the salts to the organics.....21

Figure S11. Size distribution of indole SOA at AS experiment.....22

Figure S12. Size distribution of indole SOA at AS-NO_2 experiment. 23

Figure S13. Two-dimensional thermograms of indole SOA at REF, AS, and AS-NO_2 experiments. The contour colors indicate normalized intensities.....24

List of Tables

Table S1. Top 15 major products in the gas and particle phases identified in the ind-SOA sample from REF experiment. 9

Table S2. Top 15 major products in the gas and particle phase identified in the ind-SOA sample from AS experiment. 10

Table S3. Top 15 major products in the gas and particle phase identified in the ind-SOA sample from NO_2-AS experiment. 11

S1. Measurement and data processing of aerosol mass spectrometer

The total organic particle mass and size distribution was measured by a high-resolution time-of-flight aerosol mass spectrometer (HR-ToF-AMS; Aerodyne Inc.). AMS data analysis was performed using standard software written for Igor software (V7.08, WaveMetrics, Portland, OR), including SQUIRREL (version 1.60C) and PIKA (version 1.20). For calculation of the organic particle concentration from AMS mass spectra, a collection efficiency of 0.2 – 0.5 (determined by comparison with scanning mobility particle sizer, SMPS, measurement) and an ionization efficiency of $(1.56 \pm 0.1) \times 10^{-7}$ (calibrated with 300nm ammonium nitrate particles) were used. In this study, only mass spectra in the range m/z 12 – 120 was obtained with the AMS operated in V model (mass resolution: 2000). Large ion masses had a low signal-to-noise ratio. The elemental ratios of organics including oxygen-to-carbon and hydrogen-to-carbon ratios (O/C and H/C) were calculated from the V mode data based on the 'Improved-Ambient (I-A)' method (Canagaratna et al., 2015).

S2. Measurement and data analysis of a proton transfer reaction time-of-flight mass spectrometer equipped with the chemical analysis of aerosol online particle inlet

The concentrations of indole were measured by a proton-transfer-reaction time-of-flight mass spectrometer (PTR-ToF-MS 4000, Ionicon Analytic GmbH) equipped with the CHARON (Chemical Analysis of Aerosol Online) particle inlet. Data were analyzed using PTR viewer 3.3.12. During the period of indole injection and oxidation, the PTR-ToF-MS was operated for measuring gaseous volatile organic compounds (VOCs) only. The gas phase was measured at a flow rate of 40 SCCM via a PEEK (polyether ether ketone) tube. Furthermore, a flow rate of 3.9 L min^{-1} was added to the total flow to minimize the residence time in the sampling tube. For measuring gases, the drift tube of the PTR-MS was kept at 353.15 K and 2.7 mbar, leading to an electric field (E/N) of 92 Td. In this study, we calibrated indole with pure water solvent using a liquid calibration unit (LCU-a, Ionicon Analytic GmbH), as shown in Figure S3 (Gao et al., 2022). We obtained indole sensitivity as 200 ± 21 ncps ppb^{-1} (ncps: normalized counts per second), as shown in Fig S3. The indole concentration was quantitative by using this sensitivity.

S3. Density calculation

Effective densities of indole SOA were derived from comparisons of the mass distribution from AMS and volume distribution from SMPS (Saathoff et al., 2009). Briefly, the mass distribution vs. vacuum aerodynamic diameter is from AMS. And volume distribution vs. mobility diameter is from SMPS. The density was calculated as:

$$\rho_{eff} = \frac{d_{va}}{d_m}\rho_0$$

Where $\boldsymbol{\rho}_{eff}$ is the effective density, d_{va} is the vacuum aerodynamic diameter, dm is the mobility equivalent diameter and $\boldsymbol{\rho}_0$ is the unit density (DeCarlo et al., 2004).

As shown in Figure S11, in the AS experiment, the major peaks of the size distributions were from pure indole SOA. Therefore, the seed particles do not affect the indole SOA density determination. However, in the AS-NO_2 experiment, the indole SOA density was calculated by the major peaks of coated particles as shown in Figure S12. Therefore, we used an average particle density including the AS seed and the indole SOA coating. The particle mass concentration was calculated from particle volume and average density. The seed particle mass and volume can be measured by SMPS. We obtained the pure indole SOA mass and volume. Then we calculated the pure indole SOA density.

S4. Yield calculation

The SOA yield was calculated as followed:

$$Yield = \frac{\Delta SOA}{\Delta VOC}$$

Where ΔSOA is the SOA mass concentration from SMPS. ΔVOC is a depleted indole concentration from PTR-MS (Saathoff et al., 2009; Ng et al., 2007).

S5. Wall loss calculation with aerosol dynamic model COSIMA

To calculate the wall loss of SOA in the AIDA chamber, an aerosol dynamic model COSIMA was used to simulate the formation and dynamics of aerosol (Saathoff et al., 2009). COSIMA SOA mainly simulates the physical aerosol processes including particle diffusion to the walls, sediment deposition, coagulation, condensation, evaporation, wall losses of trace gases and dilution effects due to sampling. The chamber wall is assumed to act as an irreversible sink for particles and trace gases. The detailed information about the COSIMA model was reported by Saathoff et al. (2009) and Naumann (2003). Briefly, since the indole was consumed by O_3, the intermediate products were further oxidized by O_3 and led to the formation of SOA. It is relatively difficult to know which intermediate compounds were further oxidized by OH radicals. Therefore, we simplify the oxidation process by using oxidation of indole specifically by OH radicals. The rate constant for the gas-phase reactions of indole with OH radicals was $(1.54 \pm 0.35) \times 10^{-10}$ cm^3 $molecule^{-1}$ s^{-1} (Atkinson et al., 1995). In the presence of AS-NO_2 experiments, the reaction pathways are relatively complex. During this study, we mainly used the COSIMA model to simulate the SOA from oxidation of indole at reference and seed particle experiments. The organic mass concentration, particle wall loss and gas wall loss are shown in Figure S4 and S5. The organic mass concentrations from the COSIMA model have a good agreement with the SMPS measurement. Therefore, the COSIMA model can simulate the SOA from oxidation of indole well. The yields were calculated for the initial period of the experiments, which lasted about 200 min. During this relatively short time period and due to the large size of the simulation chamber, particle losses contributed typically 4% or less to the total SOA mass. In presence of seed particle, the gas loss decreased by ~6 times.

S6. Calculation of Mass Absorption Coefficient of chromophores

Fractions of MAC corresponding to each BrC feature ($MAC_{\lambda i}$) detected in the indole SOA (Figure 4c and f) are calculated using their relative absorptions and MAC_{λ} as followed (Hettiyadura et al., 2021):

$$MAC_{\lambda} = MAC_{\lambda}\left(\frac{I_{\lambda_i} \times \Delta t_i}{I_{\lambda_i} \times \Delta t}\right)$$

where, $I_{\lambda i}$(μAU) is the averaged absorbance intensity of an individual BrC feature, i, and Δt_i (min) is its time duration. I_{λ} (μAU) is the averaged absorbance intensity across Δt =14 min of LC separation, which excludes the unresolved components eluted at 0−1 min. Unassigned fractions corresponds to total absorption from 1-15 min, other than $C_8H_7O_3N$ and $C_8H_6O_2N_2$ chromophores.

Table S1. Top 15 major products in the gas and particle phases identified in the ind-SOA sample from REF experiment.

Phases	Molecules	Mass weights	Mass fractions (%)	DBE
Gas phase	$C_8H_{16}O_5$	192.1	12.1	1
	$C_6H_{14}O_4$	150.1	9.3	0
	$C_2H_4O_3$	76.0	7.4	1
	$C_8H_6O_2N$	148.1	4.5	7
	$C_7H_4O_2N$	134.0	3.9	7
	$C_6H_{14}O_3$	134.1	2.3	0
	$C_8H_7O_3N$	165.1	1.9	6
	$C_2H_2O_4$	90.0	1.8	2
	$C_2H_4O_4$	92.0	1.7	1
	$C_4H_6O_4$	118.0	1.4	2
	$C_8H_6O_3N_2$	178.1	1.4	7
	$C_3H_6O_4N$	106.0	1.3	1
	C_8H_6ON	132.1	1.2	7
	$C_{15}H_{22}O_4$	266.2	1.2	5
	$C_{13}H_{18}O_3$	222.1	1.1	5
Particle phase	$C_8H_7O_4N$	181.1	10.0	6
	$C_8H_7O_3N$	165.1	6.2	6
	$C_8H_5O_3N$	163.0	4.8	7
	$C_8H_5O_2N$	147.0	2.6	7
	$C_2H_2O_4$	90.0	1.7	2
	$C_7H_7O_5N$	185.1	1.7	5
	$C_6H_5O_4N$	155.0	1.6	5
	$C_7H_7O_4N$	169.1	1.4	5
	$C_3H_3O_4N$	117.0	1.3	3
	$C_7H_5O_5N$	183.0	1.3	6
	$C_7H_6O_4$	154.0	1.2	5
	$C_8H_7O_5N$	197.1	1.1	6
	$C_5H_5O_4N$	143.0	1.1	4
	$C_8H_5O_4N$	179.0	1.0	7
	$C_8H_3ON_3$	157.0	0.9	9

DBE: double bond equivalent

Table S2. Top 15 major products in the gas and particle phase identified in the ind-SOA sample from AS experiment.

Phase	Molecules	Mass weights	Mass fraction (%)	DBE
Gas phase	$C_6H_{14}O_3$	134.1	17.5	6
	$C_6H_{14}O_4$	150.1	8.4	0
	$C_2H_2O_4$	90.0	5.0	2
	$C_8H_{16}O_5$	192.1	4.0	1
	$C_8H_7O_3N$	165.1	3.4	6
	$C_8H_7O_2N$	149.1	3.2	6
	$C_5H_{10}O_4$	134.1	3.2	1
	$C_5H_8O_4$	132.1	3.1	2
	$C_2H_4O_3$	76.0	2.9	1
	$C_3H_6O_4N$	120.1	1.8	1.5
	$C_8H_6O_2N$	148.1	1.8	6.5
	$C_4H_6O_4$	118.0	1.8	2
	$C_2H_4O_2$	60.0	1.7	1
	$C_3H_8O_3$	92.1	1.5	0
	$C_8H_6ON_2$	146.1	1.4	7
particle phase	$C_8H_7O_4N$	181.1	10.1	6
	$C_8H_7O_3N$	165.1	8.3	6
	$C_8H_5O_3N$	163.0	6.7	7
	$C_8H_5O_2N$	147.0	2.7	7
	$C_2H_2O_4$	90.0	2.0	2
	$C_7H_7O_5N$	185.1	1.9	5
	$C_3H_3O_4N$	117.0	1.9	3
	$C_6H_5O_4N$	155.0	1.8	5
	$C_7H_5O_5N$	183.0	1.7	6
	$C_5H_5O_4N$	143.0	1.5	4
	$C_7H_7O_4N$	169.1	1.5	5
	$C_7H_6O_4$	154.0	1.3	5
	$C_6H_5O_5N$	171.0	1.2	5
	$C_8H_7O_5N$	197.1	1.0	6
	$C_4H_4O_4$	116.0	0.9	3

DBE: double bond equivalent

Table S3. Top 15 major products in the gas and particle phase identified in the ind-SOA sample from NO_2-AS experiment.

Phase	Molecules	Mass weights	Mass fractions (%)	DBE
Gas phase	$C_8H_9O_2N_3$	179.1	12.2	6
	$C_3H_6O_3$	90.0	10.4	1
	$C_6H_{14}O_3$	134.1	9.7	0
	$C_8H_6O_2N_2$	162.1	8.7	7
	$C_6H_{14}O_4$	150.1	4.8	0
	$C_{10}H_{13}O_2N$	179.1	2.9	5
	$C_5H_{10}O_4$	134.1	2.8	1
	$C_8H_{16}O_5$	192.1	1.9	1
	$C_8H_7O_3N$	165.1	1.6	6
	$C_2H_4O_3$	76.0	1.5	1
	$C_8H_7O_2N$	149.1	1.5	6
	$C_6H_{12}O_3$	132.1	1.3	1
	$C_3H_6O_4N$	120.1	1.2	1.5
	$C_2H_4O_2$	60.0	1.2	1
	$C_{4H6}O_4$	118.0	1.0	2
particle phase	$C_8H_6O_2N_2$	162.1	76.3	7
	$C_8H_7O_4N$	181.1	3.6	6
	$C_{16}H_{12}O_4N_4$	324.1	3.4	13
	$C_3H_6O_3$	90.0	0.9	1
	$C_8H_5O_3N$	163.0	0.7	7
	$C_8H_7O_3N$	165.1	0.5	6
	$C_7H_7O_5N$	185.1	0.4	5
	$C_7H_7O_4N$	169.1	0.3	5
	$C_8H_5O_2N$	147.0	0.2	7
	$C_6H_5O_4N$	155.0	0.2	5
	$C_7H_6O_4$	154.0	0.2	5
	$C_8H_7O_5N$	197.1	0.2	6
	$C_3H_3O_4N$	117.0	0.2	3
	$C_8H_6O_5N_2$	210.1	0.2	7
	$C_5H_5O_4N$	143.0	0.2	4

DBE: double bond equivalent

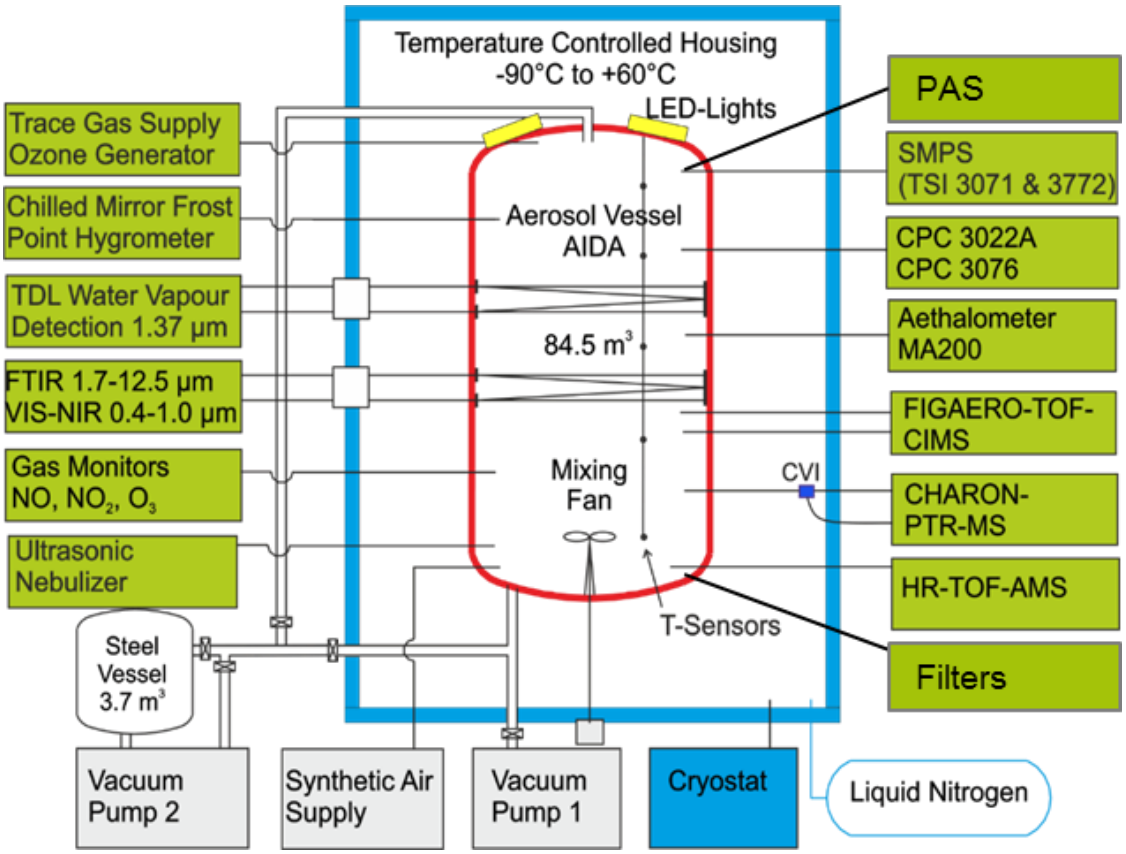

Figure S1. Schematic of the AIDA simulation chamber and its instrumentation employed for this study.

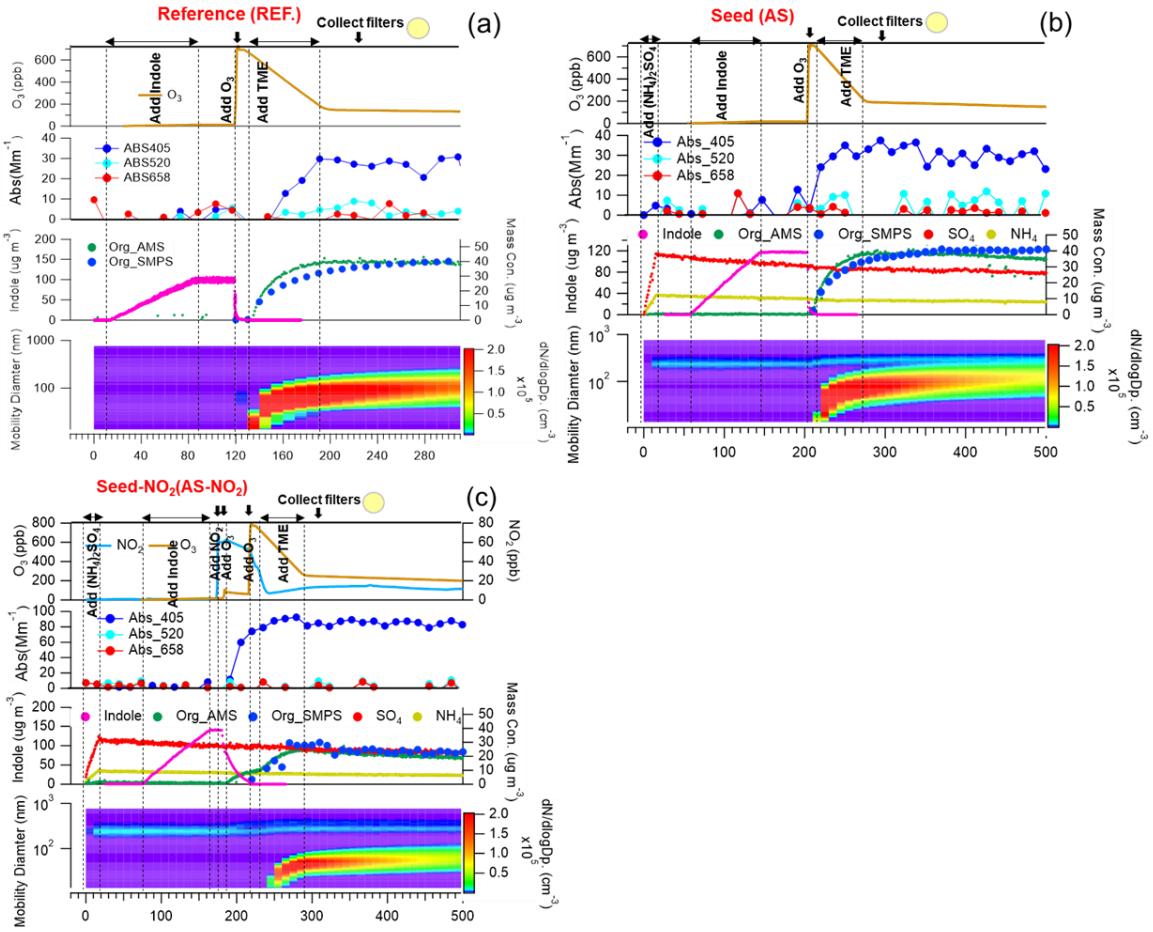

Figure S2. Evolution of trace gases, light absorption, particle mass, and size distribution of indole oxidation at REF. (a), AS (b), and AS-NO_2 (c).

As shown in Figure S2, the top panel shows the O_3 concentrations or NO_2 concentrations. The second panel shows the light absorption at three wavelengths (405, 520, 658 nm) of *ind*-SOA measured by a photoacoustic spectrometer (PAS). In the third panel, the right y-axis is indicated the aerosol mass concentrations. Organic aerosol mass concentrations were measured by an aerosol mass spectrometer (AMS) and a scanning mobility particle sizer (SMPS). The concentrations of seed particles (ammonium sulfate) were measured by AMS. The left y-axis is indicated the indole concentrations measured by a proton-transfer reaction time-of-flight mass spectrometer (PTR-MS). The final panel shows the particle size distributions measured by SMPS. The color scales are represented as particle number concentrations.

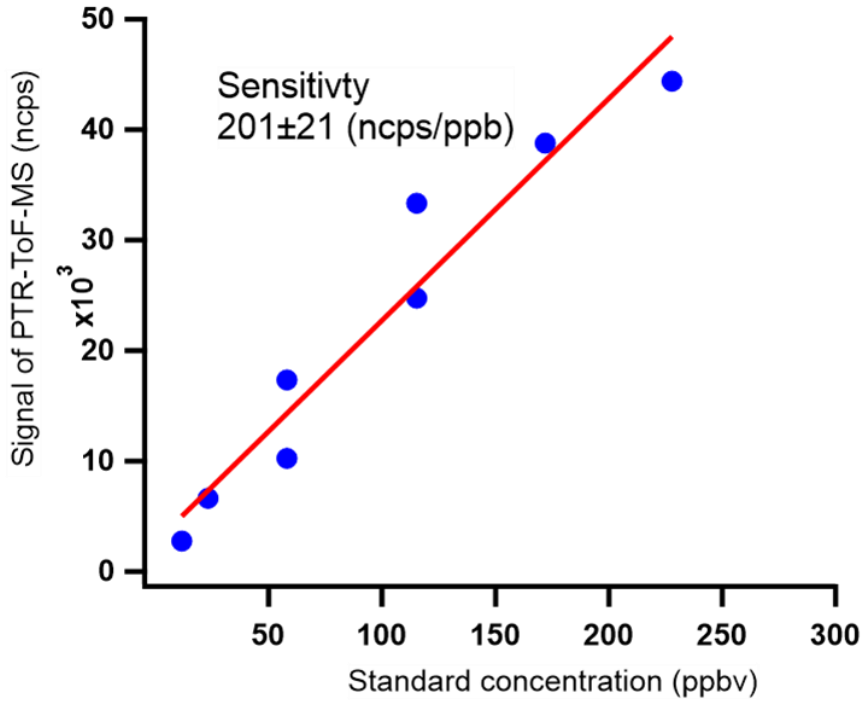

Figure S3. Indole calibration plot for PTR-MS measurements: normalized signals at 118.15 m/z (ncps) vs. generated mixing ratio (ppbv)

Figure S3 shows that the sensitivity of indole measured by PTR-MS was 201±21 (ncps/ppb). The standard concentration of indole was measured by a liquid calibration unit. ncps: normalized counts per second.

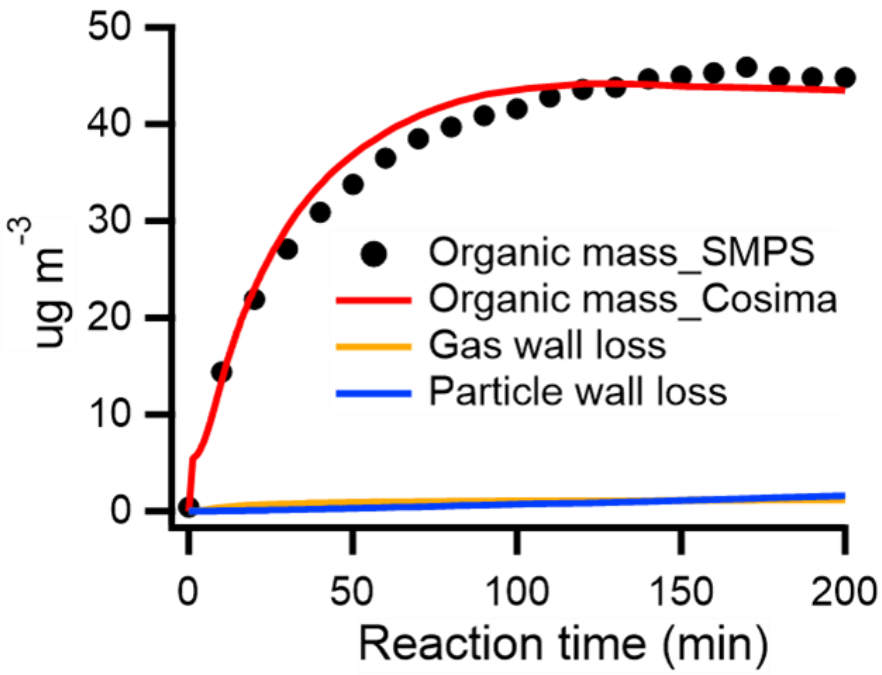

Figure S4. Organic mass concentration from SMPS measurement and COSIMA model (a reference experiment), including organic mass from SMPS (black points), organic mass from COSIMA model (red points), gas wall mass (brown line), and particle wall loss (blue line).

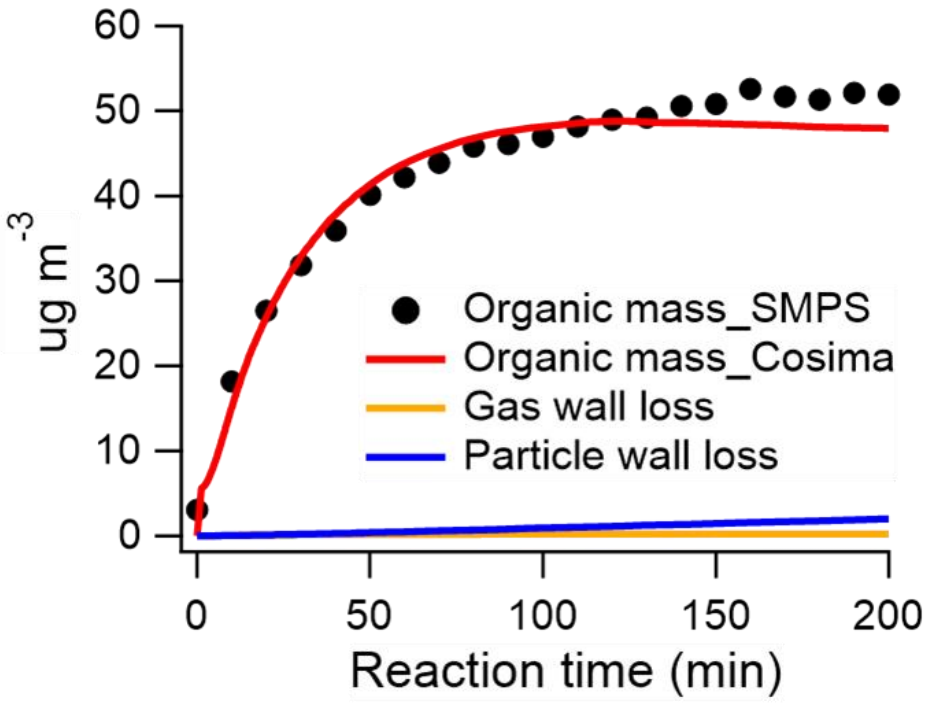

Figure S5. Organic mass concentration from SMPS measurement and COSIMA model (a seed particle experiment), including organic mass from SMPS (black points), organic mass from COSIMA model (red points), gas wall mass (brown line), and particle wall loss (blue line).

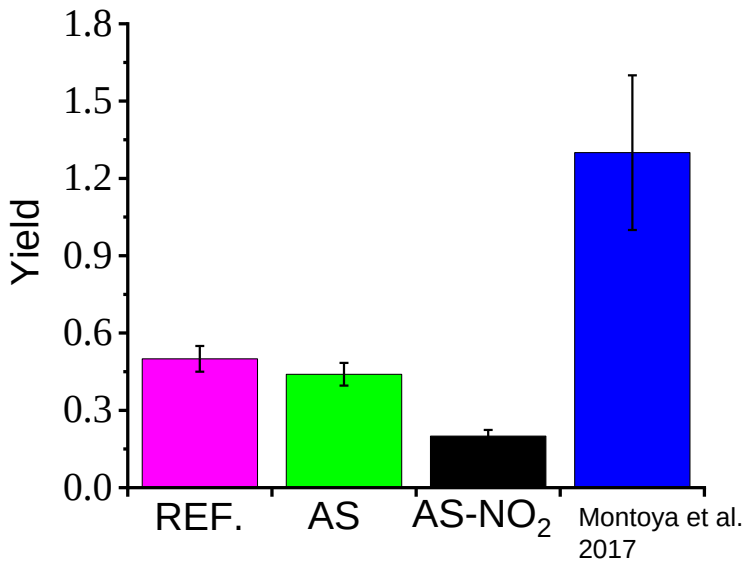

Figure S6. Yields of *ind*-SOA during stable period were recorded in the REF (pink), AS (green), and AS-NO_2 (black) experiments. The blue bar shows previously reported data by Montoya-Aguilera et al. (2017). The yields were calculated under stable periods for one hour (plateau level).

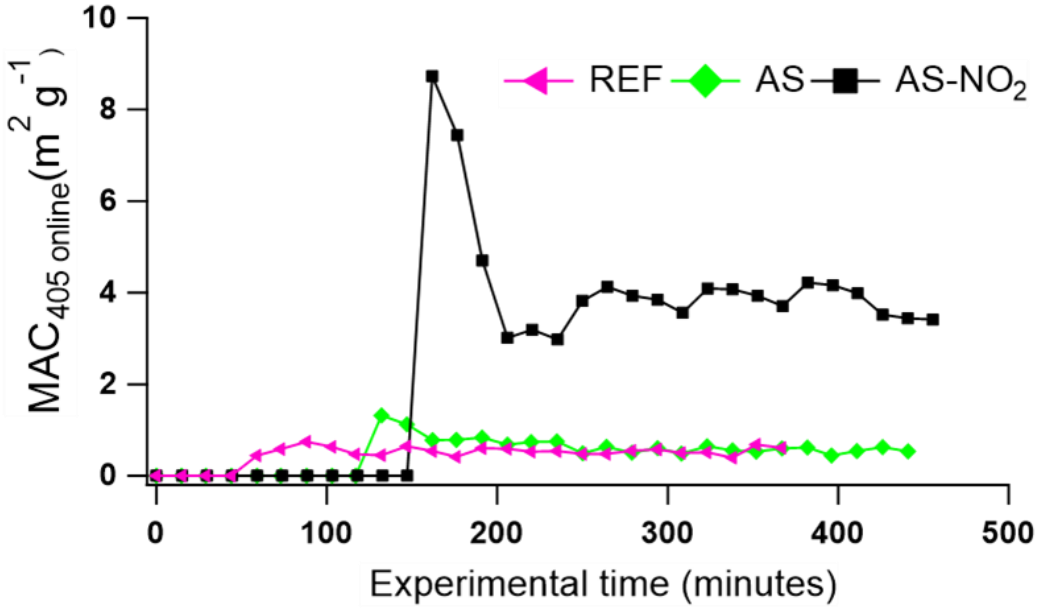

Figure S7. $MAC_{405\ online}$ of *ind*-SOA during the three experiments measured by a photoacoustic spectrometer. AS-NO_2 (black), AS (green), and REF (pink).

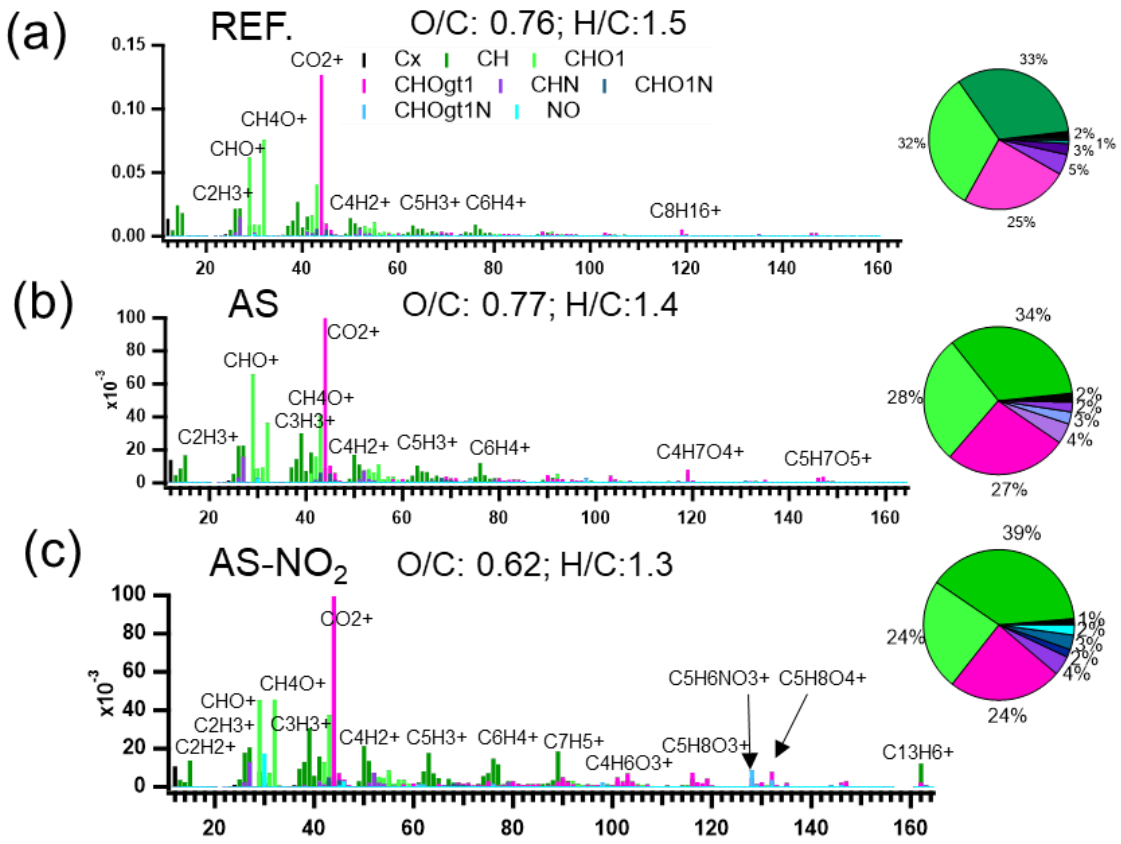

Figure S8. High-resolution AMS mass spectra of ind-SOA generated in the REF., AS, and NO_2-AS experiments. The major ion groups are grouped for clarity as Cx (black), CH+ (dark green), CHO1 (green), CHOgt1 (pink), and CHN (purple).

Figure S8 shows the mass fraction of aerosol fragmented ions from AMS measurement. Compared to the third panel (Figure S8 c) with other two panels, the *ind*-SOA in the presence of NO_2 contains higher mass fractions of large fragmented ions e.g. $C_5H_6NO_3^+$, $C_5H_8NO_4^+$, and $C_{13}H_6^+$. In addition, it shows the lowest ratio of O/C with 0.62. It indicates that *ind*-SOA in the presence of NO_2 has products of large molecular weight and low oxygenated states.

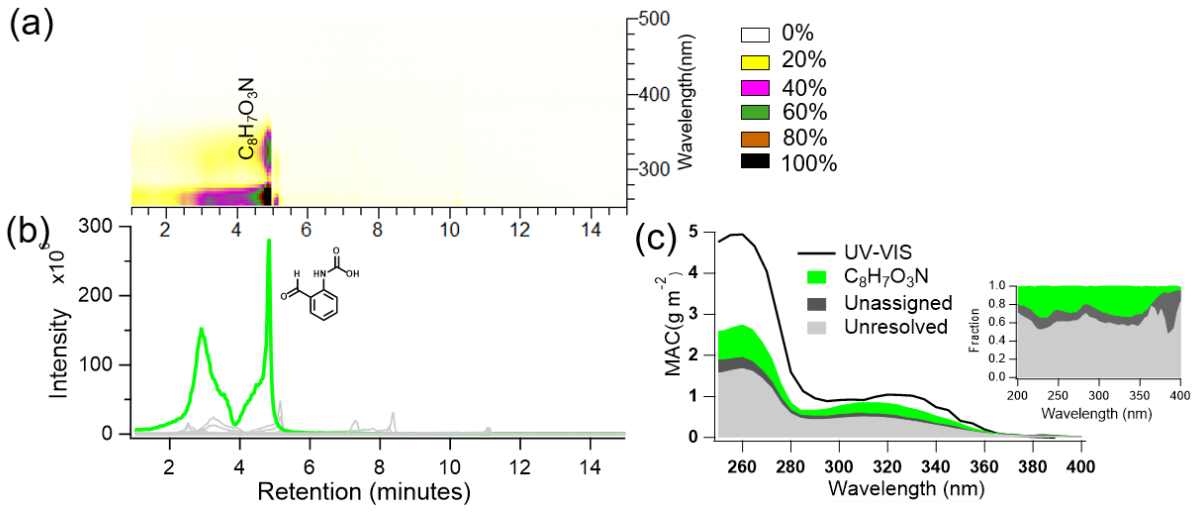

Figure S9. Molecular characteristics of individual components of *ind*-SOA identified in the reference sample. Panel (a) is the normalization of UPLC-PDA chromatograms and identified chromophores. Panel (b) shows a compilation of the selected extracted ion chromatograms (EICs) and the molecular structure of the most abundant peaks. Panel (c) shows the MAC from UV-visible spectrometer and UPLC-PDA measurement and absorption fractions. Unresolved chromophores (grey), unassigned chromophores (black), and $C_8H_7O_3N$ (green).

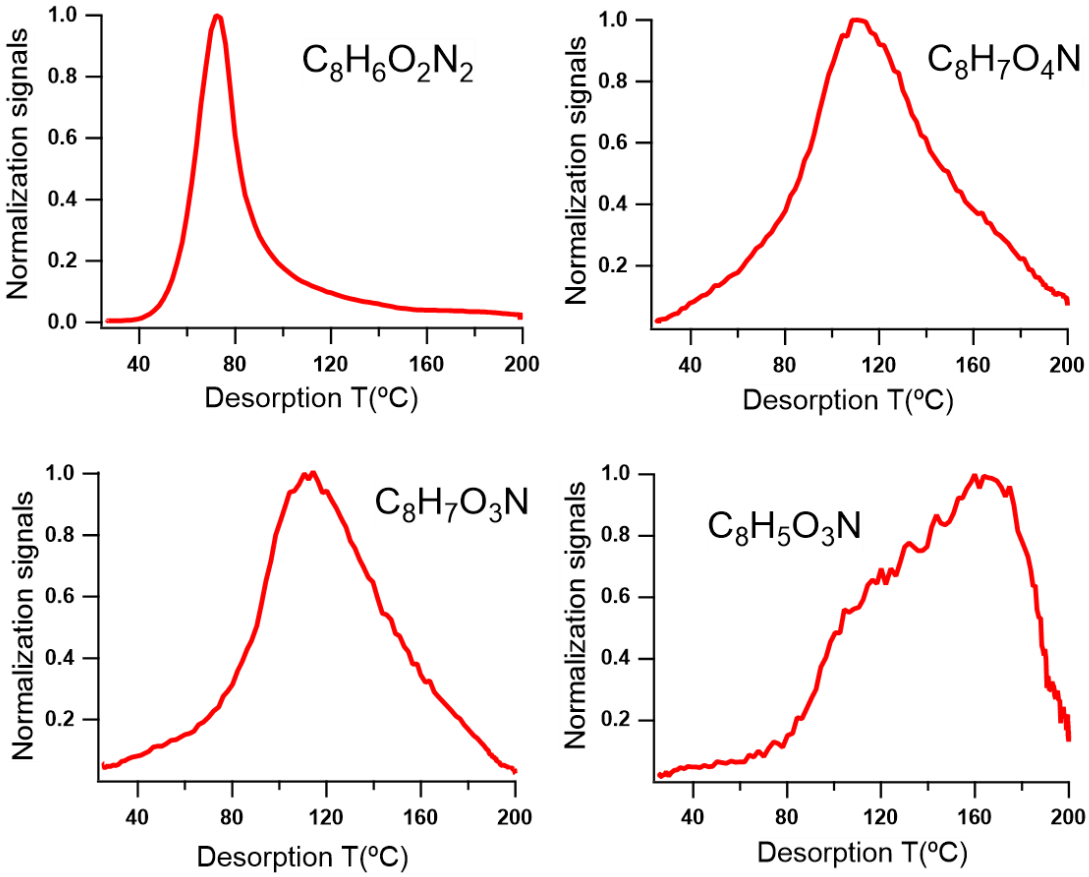

Figure S10. Thermograms of $C_8H_6O_2N_2$, $C_8H_7O_4N$, $C_8H_7O_3N$, and $C_8H_5O_3N$. Please note that broader thermograms, like those of $C_8H_7O_4N$, $C_8H_7O_3N$, and especially $C_8H_5O_3N$, may be caused by the presence of isomers of different volatility and thermal decomposition of larger molecules. Furthermore, the thermograms are also influenced by the overall composition of the matrix on the filter e.g. the ratio of the salts to the organics.

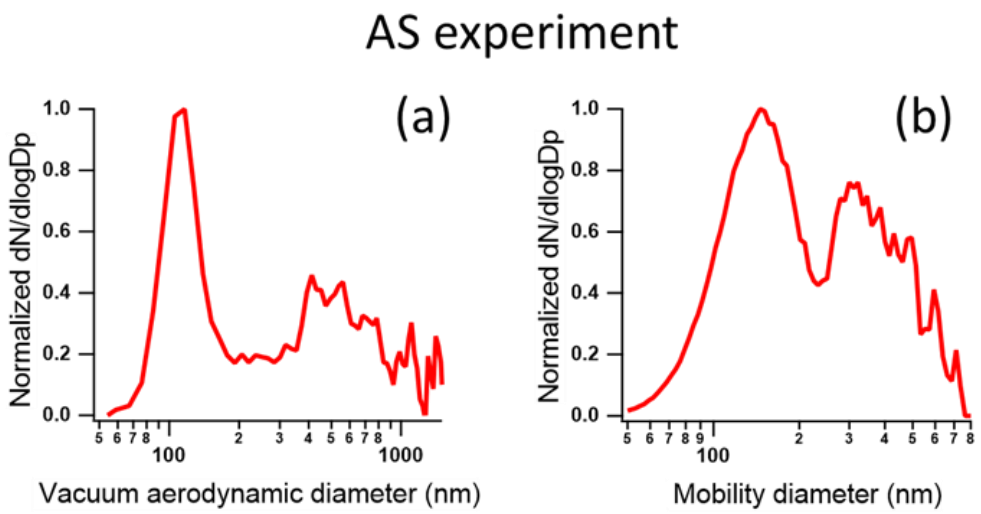

Figure S11. Size distribution of indole SOA at AS experiment.

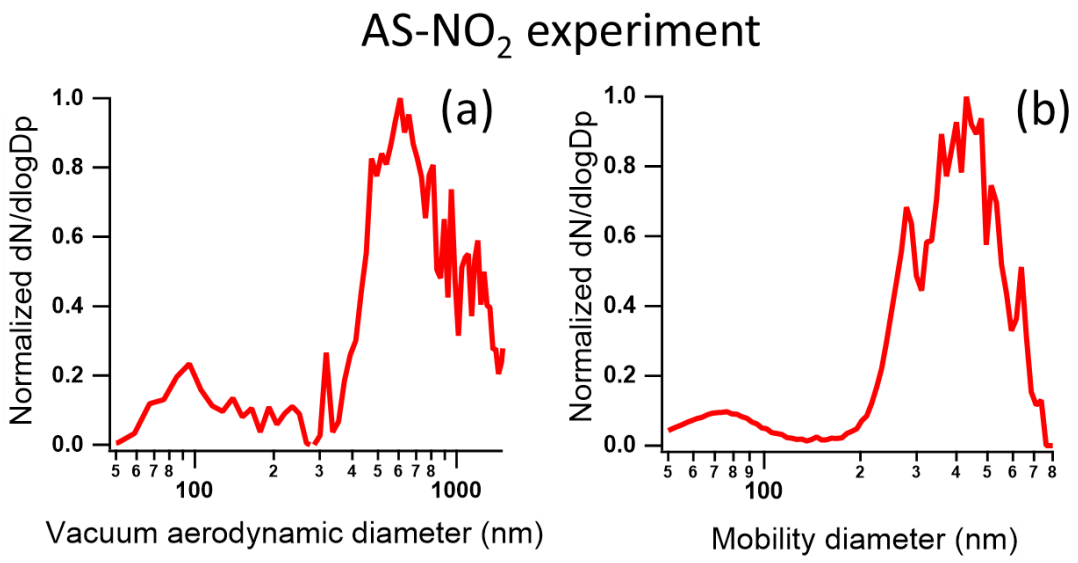

Figure S12. Size distribution of indole SOA at AS-NO_2 experiment.

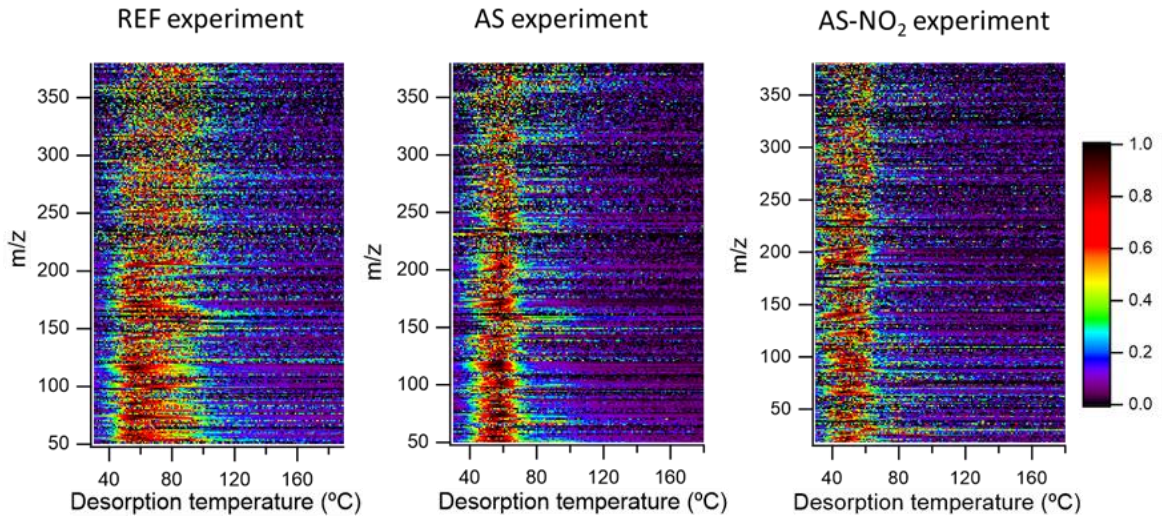

Figure S13. Two-dimensional thermograms of indole SOA at REF, AS, and AS-NO_2 experiments. The contour colors indicate normalized intensities.

Reference

Atkinson, R., Tuazon, E. C., Arey, J., and Aschmann, S. M.: Atmospheric and Indoor Chemistry of Gas-phase Indole, Quinoline, and Isoquinoline, Atmos. Environ., 29, 3423-3432, https://doi.org/10.1016/1352-2310(95)00103-6, 1995.

Canagaratna, M. R., Jimenez, J. L., Kroll, J. H., Chen, Q., Kessler, S. H., Massoli, P., Hildebrandt Ruiz, L., Fortner, E., Williams, L. R., Wilson, K. R., Surratt, J. D., Donahue, N. M., Jayne, J. T., and Worsnop, D. R.: Elemental ratio measurements of organic compounds using aerosol mass spectrometry: characterization, improved calibration, and implications, Atmos. Chem. Phys., 15, 253-272, https://doi.org/10.5194/acp-15-253-2015, 2015.

DeCarlo, P. F., Slowik, J. G., Worsnop, D. R., Davidovits, P., and Jimenez, J. L.: Particle morphology and density characterization by combined mobility and aerodynamic diameter measurements. Part 1: Theory, Aerosol Sci. Tech., 38, 1185-1205, https://doi.org/10.1080/027868290903907, 2004.

Gao, L., Song, J., Mohr, C., Huang, W., Vallon, M., Jiang, F., Leisner, T., and Saathoff, H.: Kinetics, SOA yields, and chemical composition of secondary organic aerosol from β-caryophyllene ozonolysis with and without nitrogen oxides between 213 and 313 K, Atmos. Chem. Phys., 22, 6001-6020, https://doi.org/10.5194/acp-22-6001-2022, 2022.

Montoya-Aguilera, J., Horne, J. R., Hinks, M. L., Fleming, L. T., Perraud, V., Lin, P., Laskin, A., Laskin, J., Dabdub, D., and Nizkorodov, S. A.: Secondary organic aerosol from atmospheric photooxidation of indole, Atmos. Chem. Phys., 17, 11605-11621, https://doi.org/10.5194/acp-17-11605-2017, 2017.

Hettiyadura, A. P. S., Garcia, V., Li, C., West, C. P., Tomlin, J., He, Q., . . . Laskin, A. (2021). Chemical Composition and Molecular-Specific Optical Properties of Atmospheric Brown Carbon Associated with Biomass Burning. Environ. Sci. Technol., 55, 2511–2521, https://doi.org/10.1021/acs.est.0c05883.

Naumann, K. H.: COSIMA - a computer program simulating the dynamics of fractal aerosols, Journal of Aerosol Science, 34, 1371-1397, https://doi.org/10.1016/s0021-8502(03)00367-7, 2003.

Ng, N. L., Kroll, J. H., Chan, A. W. H., Chhabra, P. S., Flagan, R. C., and Seinfeld, J. H.: Secondary organic aerosol formation from m-xylene, toluene, and benzene, Atmos. Chem. Phys., 7, 3909-3922, https://doi.org/10.5194/acp-7-3909-2007, 2007.

Saathoff, H., Naumann, K. H., Mohler, O., Jonsson, A. M., Hallquist, M., Kiendler-Scharr, A., Mentel, T. F., Tillmann, R., and Schurath, U.: Temperature dependence of yields of secondary organic aerosols from the ozonolysis of alpha-pinene and limonene, Atmos. Chem. Phys., 9, 1551-1577, https://doi.org/10.5194/acp-9-1551-2009, 2009.